

Article

A Novel Approach to Optimizing Grinding Parameters in the Parallel Grinding Process

Tengfei Yin ¹, Hanqian Zhang ^{2,3}, Wei Hang ^{4,*}  and Suet To ^{1,*} 

¹ State Key Laboratory of Ultra-Precision Machining Technology, Department of Industrial and Systems Engineering, The Hong Kong Polytechnic University, Hung Hom, Kowloon, Hong Kong SAR, China

² Guangzhou Haozhi Industrial Co., Ltd., Guangzhou 511356, China

³ School of Mechanical Engineering and Automation, Harbin Institute of Technology, Shenzhen 518055, China

⁴ College of Mechanical Engineering, Zhejiang University of Technology, Hangzhou 310014, China

* Correspondence: whang@zjut.edu.cn (W.H.); sandy.to@polyu.edu.hk (S.T.)

Abstract: Hard materials have found extensive applications in the fields of electronics, optics, and semiconductors. Parallel grinding is a common method for fabricating high-quality surfaces on hard materials with high efficiency. However, the surface generation mechanism has not been fully understood, resulting in a lack of an optimization approach for parallel grinding. In this study, the surface profile formation processes were analyzed under different grinding conditions. Then, a novel method was proposed to improve surface finish in parallel grinding, and grinding experiments were carried out to validate the proposed approach. It was found that the denominator (b) of the simplest form of the rotational speed ratio of the grinding wheel to the workpiece has a great influence on surface generation. The surface finish can be optimized without sacrificing the machining efficiency by slightly adjusting the rotational speeds of the wheel or the workpiece to make the value of b close to the ratio (p) of the wheel contact width to the cross-feed distance per workpiece revolution. Overall, this study provides a novel approach for optimizing the parallel grinding process, which can be applied to industrial applications.

Keywords: parallel grinding; surface generation; surface roughness; speed ratio; optimization



Citation: Yin, T.; Zhang, H.; Hang, W.; To, S. A Novel Approach to

Optimizing Grinding Parameters in the Parallel Grinding Process.

Processes **2024**, *12*, 493. <https://doi.org/10.3390/pr12030493>

Academic Editor: Chin-Hyung Lee

Received: 30 January 2024

Revised: 20 February 2024

Accepted: 23 February 2024

Published: 28 February 2024



Copyright: © 2024 by the authors. Licensee MDPI, Basel, Switzerland. This article is an open access article distributed under the terms and conditions of the Creative Commons Attribution (CC BY) license (<https://creativecommons.org/licenses/by/4.0/>).

1. Introduction

High-precision parts made from hard materials, such as ceramics, glasses, and single crystals, have important applications in optics, electronics, aerospace, automotive engineering, and semiconductor sectors [1–3]. The high hardness makes them difficult to machine [4]. Diamond cutting processes, including diamond turning and milling, are normally applied to machine soft materials and can reliably achieve high accuracy and good surface integrity [5–7]. By contrast, severe tool wear will occur and result in poor surface quality during diamond cutting of hard materials [8,9]. Although some field-assisted technologies, such as laser [10–12] or ultrasonic vibration [13–15] assisted technologies, have been proposed to improve the cutting performance in terms of the diamond cutting of hard materials, additional assistive devices are required, increasing the machining cost. To date, grinding is still one of the best choices and the most frequently used methods for processing hard materials, due to its simplicity, high machining quality, and cost efficiency [16]. In grinding, the workpiece material is removed by the protruded grits distributed on the working surface of the grinding wheel, and many factors, including the grinding parameters [17,18], wheel geometry [19,20], grit size [21,22], lubrication [23,24], workpiece material properties [25], dressing condition [26], and vibrations [16,27], influence the surface generation processes, determining the final surface quality. In order to optimize the grinding process to obtain good surface quality, it is important to study the surface generation process in grinding.

During the past few decades, numerous efforts have been directed towards understanding the surface formation mechanism in grinding processes. In fact, it is highly dependent on the grinding modes. Different grinding modes, such as straight surface grinding [28], external cylindrical grinding [29], internal cylindrical grinding [30], self-rotating grinding [31], parallel grinding [32], and cross grinding [33], have different geometrical motion relationships between the grinding wheel and the workpiece. Thus, the surface formation mechanism varies from one grinding mode to another. It is easily found in the literature that, in cases where both the wheel and the workpiece rotate in the grinding operations, the rotational speed ratio (the angular speed ratio) of the grinding wheel to the workpiece plays a significant role in the surface generation in the grinding processes. For instance, Patel et al. [34] conducted cylindrical plunge grinding experiments using both the integer and non-integer speed ratios and found that integer speed ratios produced a poor surface finish, while non-integer ratios yielded a complex pattern of roughness spikes. Finally, they concluded that the speed ratio had a great influence on the roughness and texture of the workpiece surfaces and the power consumption. In a self-rotating grinding process, the rotational axis of a cup wheel is parallel with that of the workpiece but offset by the distance of the wheel radius. During grinding, the cup wheel and workpiece both rotate around their own rotational axes, with the wheel feeding toward the workpiece, which can achieve a highly flat surface and is widely used in wafer grinding. Chidambaram et al. [35] built a mathematical model for predicting the grinding marks on the ground wafers and performed grinding experiments to validate the model predictions. The curvature of the grinding lines and the distance between the neighboring grinding lines were found to be highly dependent on the rotational speed ratio. Huo et al. [36] developed a grinding marks formation model for wafer grinding and conducted a series of grinding tests to verify the model and study the influences of grinding parameters including the rotational speeds of the wafer and the grinding wheel, the infeed rate, and the wheel axial run-out on the surface topography. They found that the wavelength of the surface waviness was governed only by the angular speed ratio of the grinding wheel and the silicon wafer, and choosing a proper ratio value can effectively suppress the grinding marks on the surface. Wang et al. [37] established a three-dimensional surface formation model for small ball-end diamond wheel grinding and investigated the effects of various grinding parameters on the surface characteristics. The spatial wavelength in the circumferential direction was found to only be influenced by the integer part of the rotational speed ratio, while the surface residual height was governed by the integer part and the fractional part of the speed ratio, and other grinding parameters.

Parallel grinding is the most frequently employed machining method for manufacturing complex surfaces on hard and brittle materials. The workpiece and the grinding wheel both rotate around their own rotational axes, controlled by the X-Z slides to machine the required surface form. This method has been widely used to generate flat surfaces [38], SiC Fresnel molds [39], aspheric molds [40], a noncoaxial nonaxisymmetric aspheric lens [41], and freeform surfaces [42]. The rotational speed ratio has also been found by researchers to be an important variable governing surface formation. Chen et al. [43] found that the fractional part of the rotational speed ratio of the grinding wheel to the workpiece had a significant influence on the surface roughness and surface patterns, and a phase shift (fractional part of the ratio) of 0.5 is recommended to minimize the scallop height in order to achieve a better surface finish in the parallel grinding process. Pan et al. [39] built a model for the spatial period and amplitude of the surface waviness in parallel grinding. They pointed out that the phase shift introduced by the fractional part of the non-integer rotational speed ratio was helpful in suppressing the waviness amplitude. However, the optimal values of the fractional part of the speed ratio were different in the above two works. This is because the surface roughness was not only influenced by the speed ratios but also the other grinding conditions like the feed rate. When the other grinding conditions change, the optimal value of the fractional part of the speed ratio will change accordingly; but how to determine the optimal rotational speed ratio value while considering the other

grinding conditions remains unclear. In previous works [44,45], we studied the vibration characteristics of the grinding wheel spindle and the surface formation mechanism under the spindle vibration in a parallel grinding process, and proposed a method using the reduced fraction of rotational speed ratio (not the fractional part of the decimal form) to predict the surface patterns. In this work, further analysis will be conducted to study how to optimize the grinding processes by using the reduced fraction.

The remainder of this paper is organized as follows. The surface formation mechanism will be revealed theoretically and the optimization method will be described in Section 2. The experimental details for the parallel grinding will be introduced in Section 3. Section 4 validates the method by experimental results and analysis. Conclusions will be drawn in Section 5.

2. Theoretical Analysis

In this section, the surface formation processes under different grinding parameters in parallel will be analyzed, and then an optimization method for improving the surface quality will be derived accordingly.

The configuration of the parallel grinding in this study is shown in Figure 1. The grinding wheel and the workpiece are held by the wheel spindle and the workpiece spindle, respectively. Both of them rotate in an anticlockwise direction at rotational speeds of n_1 and n_2 , respectively. The grinding wheel moves from the edge of the workpiece to the center of it at a constant cross-feed rate of v_f during the grinding process. Thus, the locus of the grinding wheel is an Archimedes spiral, and it can be expressed in the global coordinate system $O(X_w Y_w Z_w)$ of the workpiece as a function of time t :

$$\begin{cases} x_w = (R_2 - v_f t) \cos\left(\frac{2\pi n_2 t}{60}\right) \\ y_w = -(R_2 - v_f t) \sin\left(\frac{2\pi n_2 t}{60}\right) \end{cases} \quad (1)$$

where R_2 is the radius of the workpiece.

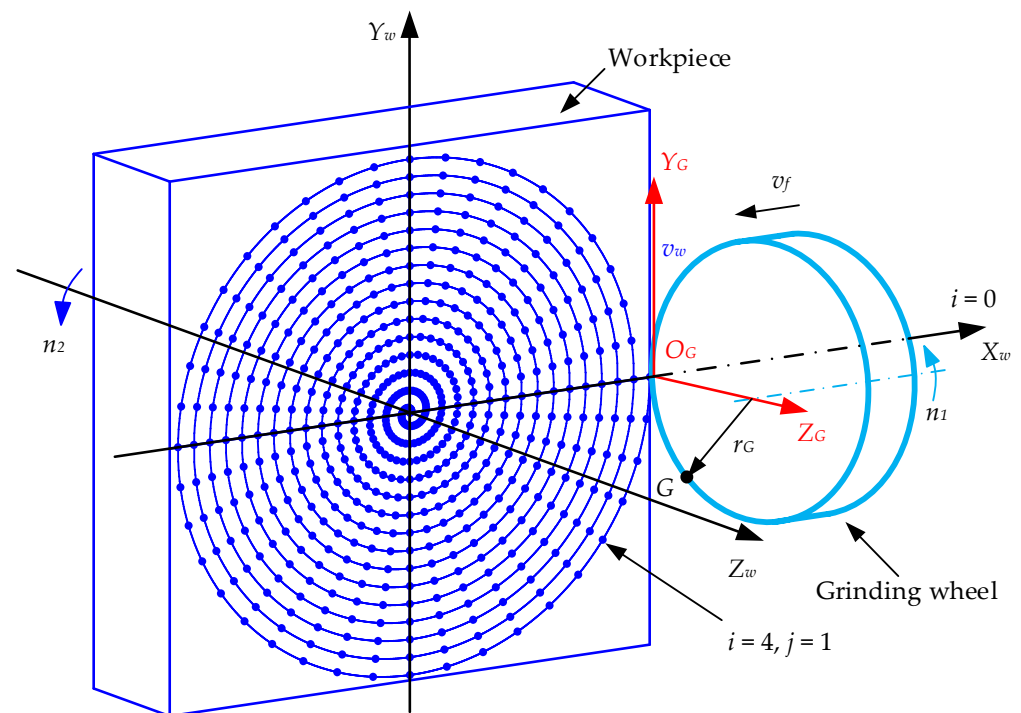


Figure 1. The configuration of the parallel grinding process.

It can also be written as:

$$\begin{cases} x_w = (R_2 - v_f \frac{30\theta}{\pi n_2}) \cos\theta \\ y_w = -(R_2 - v_f \frac{30\theta}{\pi n_2}) \sin\theta' \end{cases} \quad (2)$$

where θ is the rotation angle of the workpiece from $t = 0$ to t .

In the workpiece coordinate system $O(X_w Y_w)$, the workpiece surface is discretized into certain elements in the circumferential direction and the radial direction according to the two-dimensional locus of the workpiece expressed in Equations (1) or (2). The number of sections in the circumferential direction (N_c) and radial direction (N_r) can be calculated as:

$$\begin{cases} N_c = \frac{2\pi}{\Delta\theta} \\ N_r = \frac{R_2}{s} \end{cases}, \quad (3)$$

where $\Delta\theta$ is the angle interval in the circumferential direction, and s is the feeding distance per when the workpiece completes one revolution.

Therefore, the two-dimensional workpiece surface can be expressed in the discrete form as:

$$\begin{cases} x_w(i, j) = \left[R_2 - i \frac{R_2}{N_c N_r} - (j - 1) \frac{R_2}{N_r} \right] \cos(i\Delta\theta) \\ y_w(i, j) = - \left[R_2 - i \frac{R_2}{N_c N_r} - (j - 1) \frac{R_2}{N_r} \right] \sin(i\Delta\theta) \end{cases} \quad \begin{matrix} \text{for } i = 0, 1, 2 \dots N_c \\ j = 1, 2, 3 \dots N_r \end{matrix} \quad (4)$$

In the grinding process, a series of scallops are often generated due to the wheel run-out, wheel spindle vibration, or the ununiform grit height distribution on the wheel surface. The grinding wheel spindle vibration will produce the same vibration to the center of the grinding wheel, and then the trajectory paths of grits during rotation of the grinding wheel change correspondingly. As a result, the vibration will be copied onto the workpiece, producing a wavy surface [16,46]. Similarly, wheel run-out can also produce ups and downs on the ground surface, and an analysis of the influence of the wheel run-out on the wavy surface formation can be found in [39,47]. The trajectories of ununiform size and the distribution of grains on the grinding wheel surface may form a wavy surface and the corresponding analyses can be referred to in [16,46].

It is accepted in previous studies that the scallop height increases with the radial distance of the workpiece since a larger distance leads to a higher linear velocity when the workpiece spindle is operated at a constant rotational speed. If the scallop height is w_v at a certain radial distance, the surface profile can be simplified as:

$$h(i, j) = w_v \left(1 - \left| \cos\left(\frac{n_1}{2n_2}(i\Delta\theta + 2\pi(j-1))\right) \right| \right). \quad (5)$$

How to calculate the value of w_v is not the focus of this study, but this can be found in [16,39,45]. It should be noted that the surface profile calculated using Equation (5) is just a simplified form, describing the primary characteristics of the profile. Some secondary characteristics of the final generated surface profile induced by the uneven height and distribution of grits could not be considered in Equation (5).

In our previous research [45], a method using the lowest form of the rotational speed ratio of the grinding wheel to the workpiece has been proposed to reveal the formation mechanisms of the scallop waviness patterns of the workpiece surface in parallel grinding. In this method, b and d are defined as:

$$\frac{d}{b} = \frac{n_1}{n_2}. \quad (6)$$

By reducing the fraction (n_1/n_2) to lowest terms, the corresponding denominator and numerator are the values of b and d , respectively. In other words, b and d are the smallest integers that satisfy Equation (6).

Figure 2 shows the simulated surface profiles during three workpiece revolutions. In the simulation, the scallop height w_v of the wavy surface profile is set to be $1\ \mu\text{m}$, and the contact width of the grinding wheel is considered to be less than the feeding distance per workpiece revolution (s). $b = 1$ means that the rotational speed of the grinding wheel is an integer (d) times that of the workpiece. Thus, when the workpiece completes one cycle, a wavy surface profile with d periods is generated. In addition, since the rotational speed ratio is an integer, the surface profiles generated during each workpiece revolution are in the same angular position, as shown in Figure 2a. The red point denotes the center of the workpiece. It is clearly seen that the peaks of surface profiles generated during different workpiece revolutions are positioned at the same angular coordinate, as indicated by the green line with an arrow. However, if $b \neq 1$, the rotational speed ratio will not be an integer. Phase shift occurs during every adjacent workpiece revolution, as shown in Figure 2b.

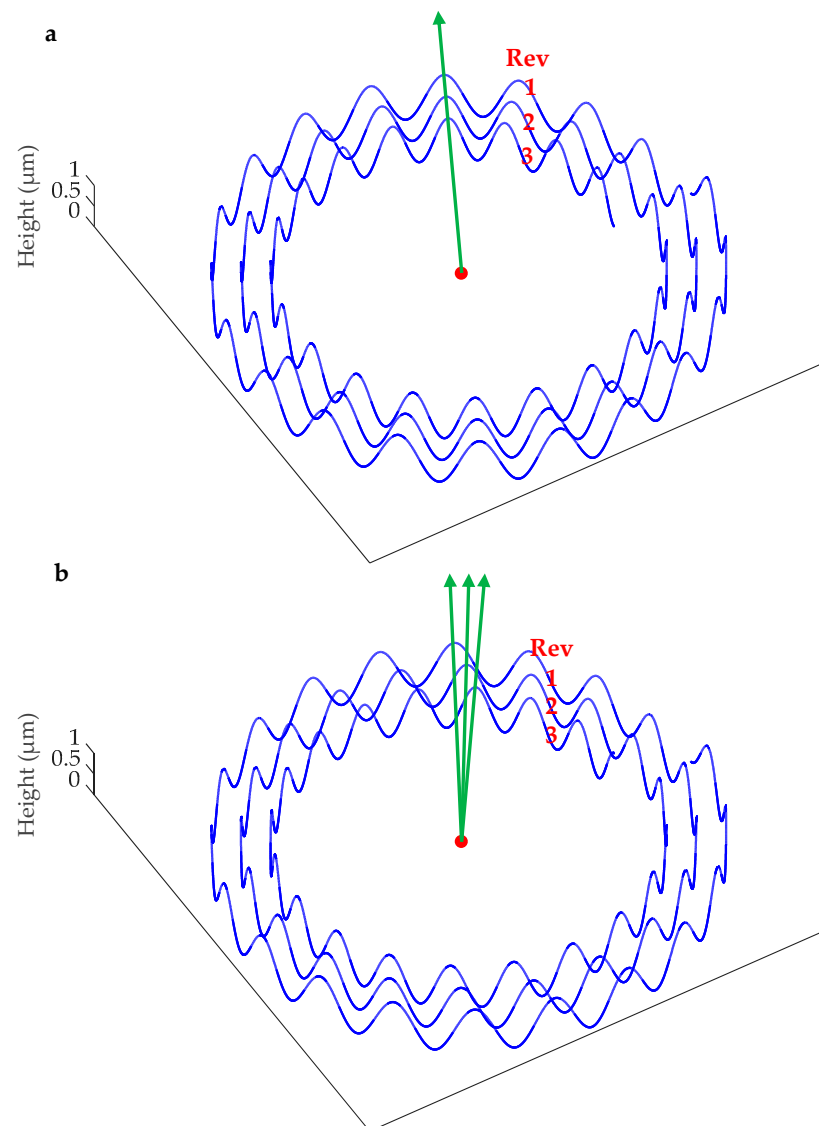


Figure 2. The wave surface profile generation (a) $b = 1$; and (b) $b \neq 1$.

In the actual grinding process, the cross-feed rate v_f is often selected to be small enough to make sure that the feed distance per workpiece revolution is smaller than the contact width of the workpiece. In this situation, there exists a primary grinding zone and a secondary grinding zone, as shown in Figure 3. The primary zone corresponds to the feed distance per workpiece revolution (s). The secondary grinding zone is introduced since the contact width is larger than s .

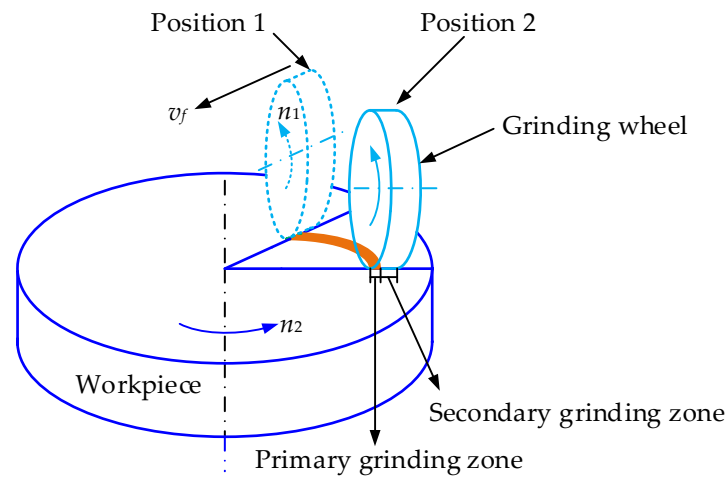


Figure 3. The primary grinding zone and the secondary grinding zone.

Figure 4 illustrates the surface profile generation due to the existence of the secondary grinding zone. It can be clearly seen that the surface profile generated by the primary grinding zone (indicated by the blue line) will be changed by the secondary grinding zone (the red line). If the ratio of the grinding wheel contact width to the feeding distance per workpiece is p , the width ratio of the secondary grinding zone to the primary grinding zone will be $p - 1$, which means that the surface profile generated by the primary grinding zone in the j -th workpiece revolution will be changed by the following $p - 1$ workpiece revolutions if phase shift exists (i.e., $b \neq 1$). This effect is called the overlapping effect.

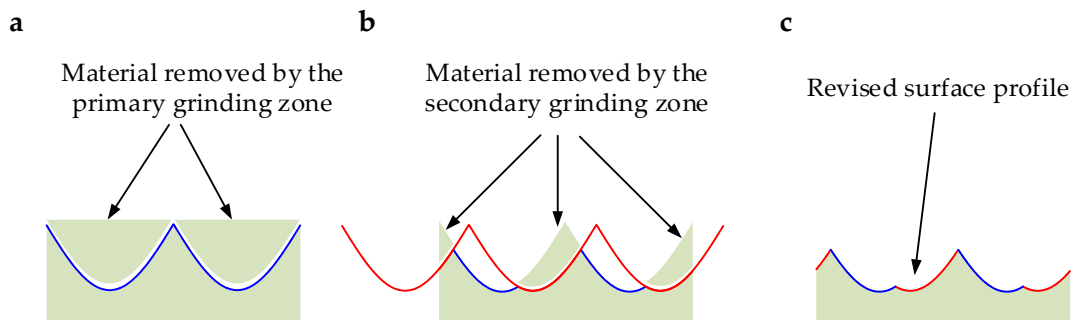


Figure 4. The surface profile generation due to the existence of the secondary grinding zone.

It can be observed that the overlapping effect leads to a reduction of the scallop height of the surface profile, which indicates that $b \neq 1$ can produce a better surface finish in comparison to $b = 1$. The degree of the overlapping effect which is related to the value of b determines how much reduction the scallop height experiences. Thus, how to select the value of b corresponding to the best surface finish is very important, and can be a way to optimize the parallel grinding process.

Figure 5 shows the surface profile generation process at different b values. p is set to be 3, thus the surface profile generated by the primary grinding zone in the first workpiece revolution will be influenced by the following two revolutions. In Figure 5a–d, $b = 5, 4, 3$, and 2, respectively. It can be seen that the scallop height decreases first and increases as the value of b decreases. More importantly, it achieves the minimum when $b = p$ (3). In Figure 5, the phase shift (fractional part of the rotational speed ratio) is $1/5, 1/4, 1/3$, and $1/2$. It should be noted that $b = p$ still corresponds to the minimal scallop height, even if the phase shift is changed to $2/5, 3/5, 4/5, 3/4$, and $2/3$. In Figure 5, $p = 3$ is just an example; if p is changed to other values, the conclusion that $b = p$ produces the minimal scallop height is still valid.

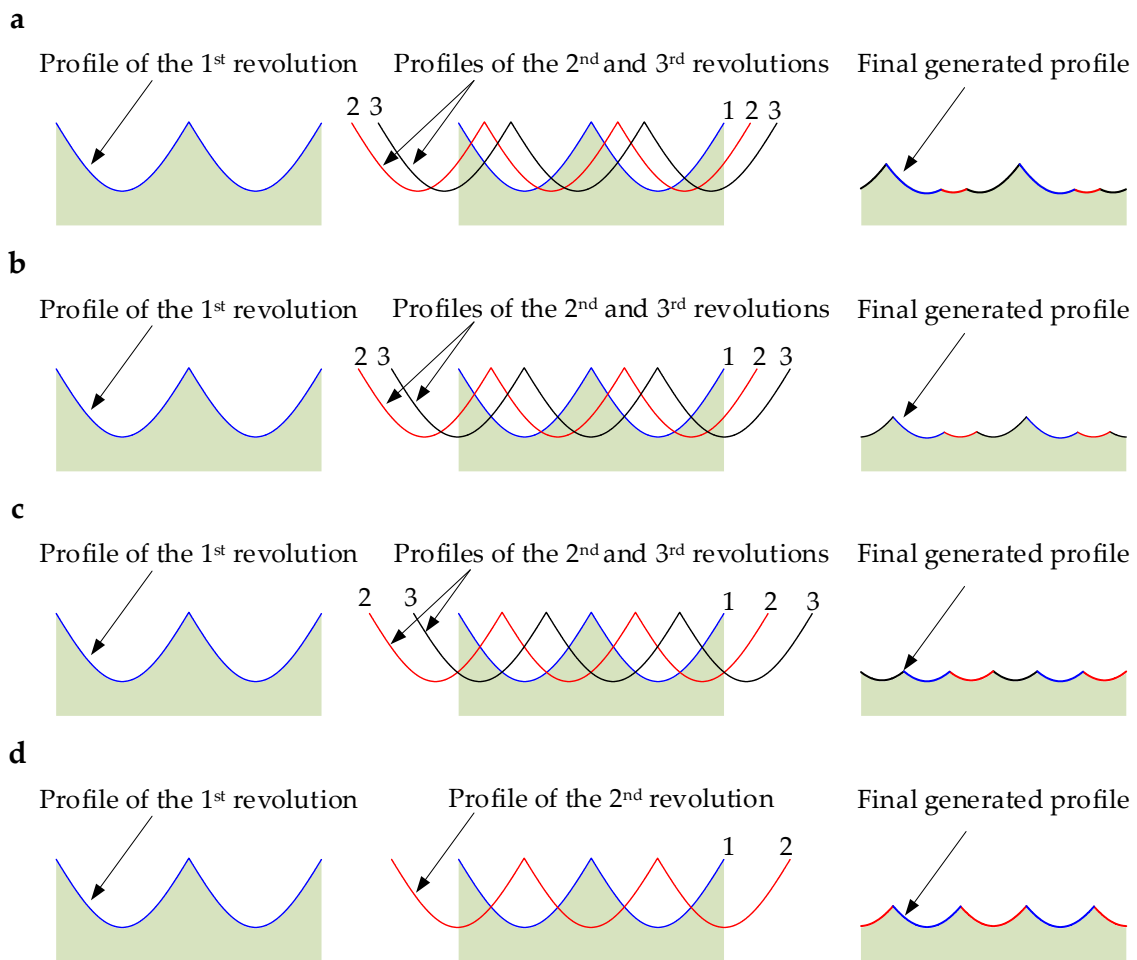


Figure 5. The surface profile generation process at different b values. (a) $b = 5$; (b) $b = 4$; (c) $b = 3$; and (d) $b = 2$.

3. Experimental Details

To validate the theoretical analysis in Section 2, a series of grinding experiments were conducted at different rotational speed ratios corresponding to different b values, and the measured ground surface profiles were analyzed.

The experimental setup is shown in Figure 6. Grinding experiments were performed on an ultra-precision grinding machine (Nanotech 450UPL, Moore Nanotechnology Systems, LLC, Swanzey, NH, USA). The workpiece with a fixture was mounted on the workpiece spindle through a vacuum chuck, and the grinding wheel was held by the wheel spindle. Both spindles were supported by ultra-precision aerostatic bearings to provide precise rotation motions. They rotated in an anticlockwise direction in the grinding operation. The grinding depth was controlled by the Z slide and the cross-feed motion was controlled by the X slide. The workpiece material was reaction-bonded silicon carbide sheets with a dimension of $8 \text{ mm} \times 8 \text{ mm} \times 5 \text{ mm}$. A resin-bonded diamond grinding wheel with a mesh number of 325# was employed in the experiments. The diameter and width of the grinding wheel were 20 mm and 5 mm, respectively. The grinding wheel had a sharp edge whose measured radius was approximately $30 \mu\text{m}$, as shown in Figure 6. The minimum quantity lubrication was applied to all the grinding tests.

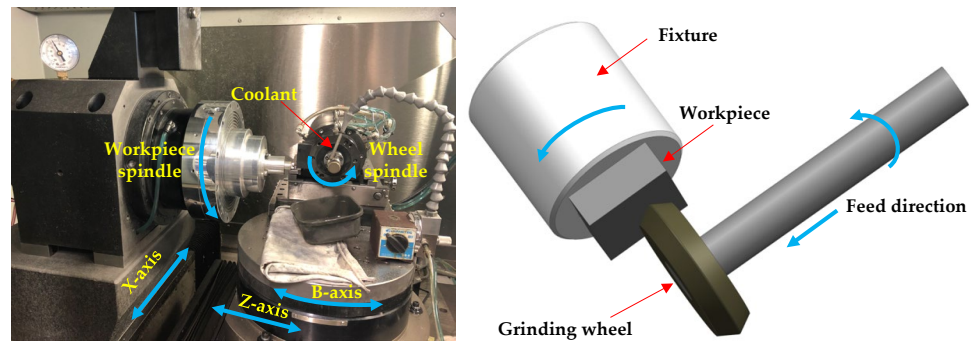


Figure 6. Experimental setup with an enlarged view of the geometrical motion relationship between the workpiece and the grinding wheel.

The values of the grinding parameters are shown in Table 1. The cross-feed rate, the grinding depth, and the workpiece spindle speeds were $8 \text{ mm} \cdot \text{min}^{-1}$, $2 \text{ }\mu\text{m}$, and 2000 rpm, respectively. The grinding wheel speeds were set to be 40,000 rpm, 40,200 rpm, 40,400 rpm, 40,667 rpm, and 41,000 rpm. Thus, the corresponding b values are 1, 10, 5, 3, and 2, respectively. For the grinding wheel spindle, the actual rotational speed deviated slightly from the preset one. However, by carefully adjusting the preset values in the experiments, the actual rotational speeds could be ensured to be almost consistent with the values listed in Table 1 within an error of less than 1 rpm.

Table 1. Grinding conditions.

Parameters	Values
Cross-feed rate	$8 \text{ mm} \cdot \text{min}^{-1}$
Grinding depth	$2 \text{ }\mu\text{m}$
Workpiece spindle speed	2000 rpm
Grinding wheel spindle speed	40,000 rpm, 40,200 rpm, 40,400 rpm, 40,667 rpm, 41,000 rpm

Before each grinding test, truing and dressing operations for the grinding wheel were performed on machine to keep the grinding wheel surface fresh and reduce the influences of the grinding wheel wear. Also, the balancing operations were performed carefully for both spindles, because the mass imbalance-induced vibration can have a great influence on surface generation in grinding. After grinding, the workpieces were removed from the fixture and cleaned using alcohol. Then, the surface topographies of the workpieces were measured by an optical surface profiler (Zygo@ Nexview, Zygo Corporation, Middlefield, CT, USA) for analysis.

4. Experimental Results and Discussion

The three-dimensional surface topographies of the workpieces at different grinding wheel spindle speeds, which corresponded to different b values, were obtained by Zygo@ Nexview. The scallop height was different at different radial distances of the workpieces; that was, a larger radial distance produced a higher scallop height due to a higher linear velocity in the parallel grinding processes. Thus, the surface roughness was not uniform along the radial direction of the workpiece. In this study, the surface profiles in the circumferential direction at the radial distance of 1.5 mm were extracted from the three-dimensional surface height data from the measurement results for analyzing the variation of the surface roughness with the value of b .

Figure 7 shows the surface profiles in the circumferential direction for different b values. It can be seen that the scallop height was the highest when $b = 1$ among these five profiles. This is because there was no phase shift when $b = 1$, and the surface profiles generated by the primary grinding zone were not influenced by the secondary grinding zone. If $b \neq 1$, the phase shift occurred between the profiles generated by neighboring

workpiece revolutions, resulting in the overlapping effect, which contributed to a reduction of the scallop height. In the experiment, the ratio (p) of the grinding wheel contact width to the feeding distance was close to 3. It can be seen that the scallop height decreased first and then increased with the decreasing value of b . When $b = p$, it reached the minimum.

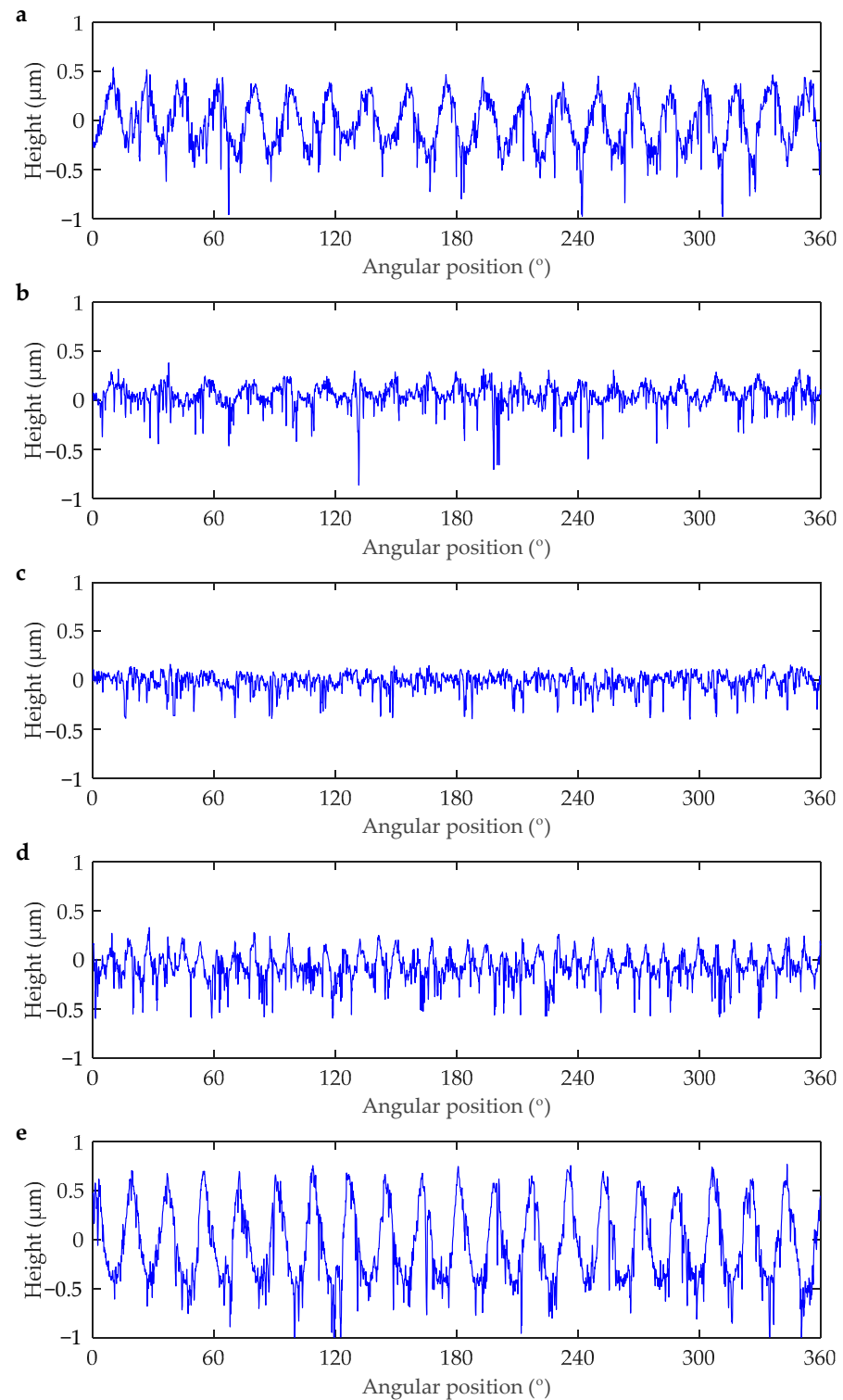


Figure 7. The measured surface profiles of the workpieces at the radial distance of 1.5 mm at different b values (a) 10; (b) 5; (c) 3; (d) 2; and (e) 1.

In addition, when $b = 1$, the period number of the surface profile was 20, which was equal to the value of d . When $b < p$, the period number would increase due to the overlapping effect (for example, in Figure 7d, the period number increased to 41); however, it was still equal to the value of d . When $b > p$, the period number would change very slightly (less than 1).

The roughness values of the above surface profiles shown in Figure 7 were also calculated for analysis, in which the arithmetic roughness (R_a) and the root-mean-square roughness (R_q) were adopted. Figure 8 shows the variation of the surface roughness including R_a and R_q with the value of b . The measured surface profiles are in the circumferential direction that is perpendicular to the feed direction. The data of the surface profiles are extracted from the three-dimensional surface data measured by the optical surface profiler. The length of the surface profiles is 9.4248 mm and there are 6390 measurement points along the circumferential direction. It can be seen that the value of b has a great influence on the roughness of the surface profiles of the workpiece. When b is close to p , both R_a and R_q are the minimum, though the values of R_q are slightly larger than those of R_a for all the cases.

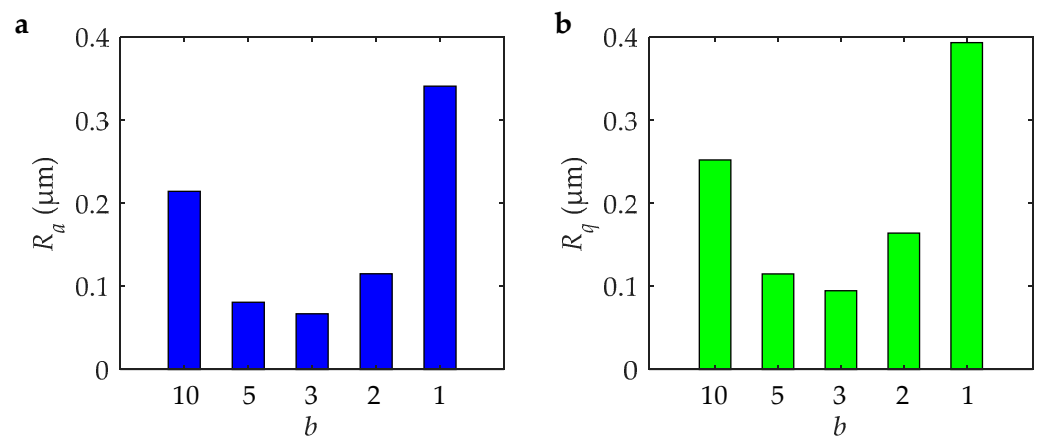


Figure 8. The variation of the roughness of the surface profiles of the workpieces with the value of b . (a) R_a and (b) R_q .

In addition, to evaluate the influence of b values on the whole surfaces, the roughness values of the whole surfaces of the workpieces are obtained, including the arithmetic roughness (S_a) and the root-mean-square roughness (S_q) at different values of b , as shown in Figure 9. Similar to the results of the roughness of the surface profiles in the circumferential direction described in Figure 8, the root-mean-square roughness (S_q) values are slightly higher than the arithmetic roughness (S_a) values for all the b values. It can also be found that the roughness values of the whole surfaces are higher than those of the surface profiles in the circumferential direction at the radial position of 1.5 mm by comparing Figures 8 and 9. More importantly, b values have the same influence on the roughness of the whole surface, that is, the roughness decreases first and increases with b . When b is close to p , the roughness can reach the minimum. This indicates that the grinding process can be optimized in terms of surface roughness by selecting an appropriate b value.

Therefore, adjusting the rotational speed of the workpiece or that of the grinding wheel to regulate the value of b to make it close to the ratio (p) of the grinding wheel contact width to the cross-feed per workpiece revolution can be a convenient way to optimize the parallel grinding process for achieving a better surface finish without compromising the machining efficiency.

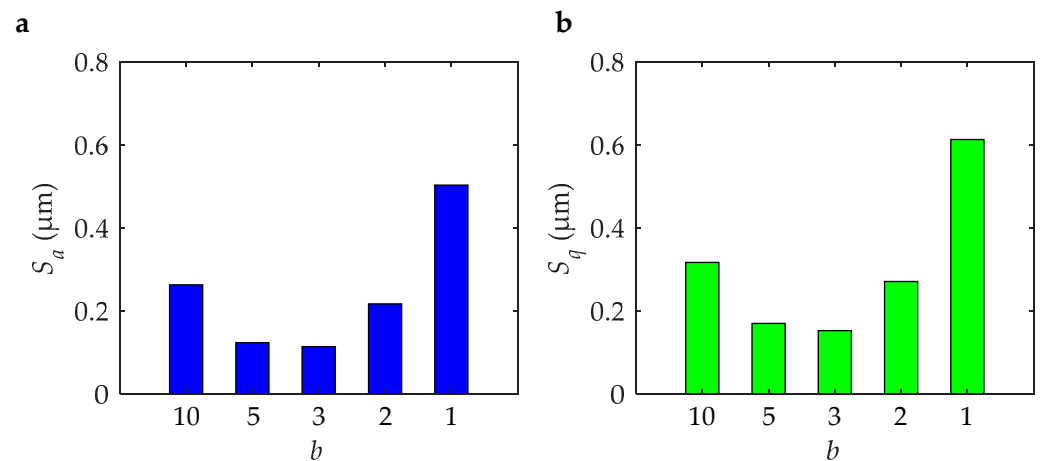


Figure 9. The variation of the roughness of the whole surfaces of the workpieces with the value of b . (a) S_a and (b) S_q .

In the grinding operation, it is generally accepted that the smaller workpiece speeds and higher grinding wheel speeds can produce a better surface finish if the overlapping effect does not exist. However, it should be noted that the grinding wheel speeds close to the natural frequency of the grinding spindle system may deteriorate the surface roughness due to the resonance [16]. After the rotational speed values of the grinding wheel spindle and the workpiece spindle are roughly determined, the overlapping effect can be introduced to decrease the surface roughness. By carefully adjusting the speed values to make the b value close to the ratio p , the optimal surface roughness can be achieved.

5. Conclusions

In this study, the surface generation processes were analyzed at different grinding conditions for parallel grinding, and a novel approach to optimizing the surface finish was proposed. Finally, grinding experiments were conducted to verify the effectiveness of the approach. The main conclusions are drawn as follows:

- (1) There exists a primary grinding zone and a secondary grinding zone when the grinding wheel contact width is larger than the feed per workpiece revolution.
- (2) The denominator (b) of the simplest form of the rotational speed ratio of the grinding wheel to the workpiece has a great influence on surface generation. When $b \neq 1$, the phase shift occurs between surface profiles generated by neighboring workpiece revolutions, introducing the overlapping effect. The surface profile generated by the primary grinding zone will be revised by the secondary grinding zone.
- (3) The overlapping effect makes a contribution to the reduction of the scallop height on the ground surface. The surface finish can be optimized by adjusting the rotational speeds of the workpiece spindle or the grinding wheel spindle to make the value of b close to the ratio (p) of the wheel contact width to the feed per workpiece revolution.

In summary, the proposed approach for optimizing the parallel grinding process is an effective way to improve the surface quality of workpieces without compromising the machining rate, which can be applied to industrial applications.

Author Contributions: Conceptualization, T.Y.; methodology, T.Y.; software, T.Y.; validation, T.Y., H.Z. and W.H.; formal analysis, T.Y. and H.Z.; investigation, T.Y., H.Z., W.H. and S.T.; resources, S.T.; data curation, T.Y. and S.T.; writing—original draft preparation, T.Y.; writing—review and editing, T.Y. and S.T.; visualization, T.Y.; supervision, S.T.; project administration, S.T.; funding acquisition, S.T. and W.H. All authors have read and agreed to the published version of the manuscript.

Funding: This research was funded by National Key Research and Development Program of China (Grant No. 2023YFE0202900) and International Science and Technology Cooperation Project of Guangzhou Development District/Huangpu District (Project No. 2020GH05). The work was also

partially supported by the funding support to the State Key Laboratories in Hong Kong from the Innovation and Technology Commission (ITC) of the Government of the Hong Kong Special Administrative Region (HKSAR), China. The authors also would like to thank the Research Committee of The Hong Kong Polytechnic University.

Data Availability Statement: Data are contained within the article.

Conflicts of Interest: Hanqian Zhang was employed by Guangzhou Haozhi Industrial Co., Ltd., Guangzhou, China. The remaining authors declare that the research was conducted in the absence of any commercial or financial relationships that could be construed as a potential conflict of interest.

References

- Brinksmeier, E.; Mutlugünes, Y.; Klocke, F.; Aurich, J.; Shore, P.; Ohmori, H. Ultra-precision grinding. *CIRP Ann.* **2010**, *59*, 652–671. [\[CrossRef\]](#)
- Huang, H.; Li, X.; Mu, D.; Lawn, B.R. Science and art of ductile grinding of brittle solids. *Int. J. Mach. Tools Manuf.* **2021**, *161*, 103675. [\[CrossRef\]](#)
- Zhao, G.; Zhao, B.; Ding, W.; Xin, L.; Nian, Z.; Peng, J.; He, N.; Xu, J. Nontraditional energy-assisted mechanical machining of difficult-to-cut materials and components in aerospace community: A comparative analysis. *Int. J. Extrem. Manuf.* **2023**, *6*, 022007. [\[CrossRef\]](#)
- Chen, H.; Wu, Z.; Hong, B.; Hang, W.; Zhang, P.; Cao, X.; Xu, Q.; Chen, P.; Chen, H.; Yuan, J. Study on the affecting factors of material removal mechanism and damage behavior of shear rheological polishing of single crystal silicon carbide. *J. Manuf. Process.* **2024**, *112*, 225–237. [\[CrossRef\]](#)
- Du, H.; Yin, T.; Yip, W.S.; Zhu, Z.; To, S. Generation of structural colors on pure magnesium surface using the vibration-assisted diamond cutting. *Mater. Lett.* **2021**, *299*, 130041. [\[CrossRef\]](#)
- Zhao, L.; Zhang, J.; Zhang, J.; Hartmaier, A.; Sun, T. Numerical simulation of materials-oriented ultra-precision diamond cutting: Review and outlook. *Int. J. Extrem. Manuf.* **2023**, *5*, 022001. [\[CrossRef\]](#)
- Wang, J.; Wang, Y.; Zhang, G.; Xu, B.; Zhao, Z.; Yin, T. Fabrication of Polymethyl Methacrylate (PMMA) Hydrophilic Surfaces Using Combined Offset-Tool-Servo Flycutting and Hot Embossing Methods. *Polymers* **2023**, *15*, 4532. [\[CrossRef\]](#)
- Zhang, Z.; Yan, J.; Kuriyagawa, T. Study on tool wear characteristics in diamond turning of reaction-bonded silicon carbide. *Int. J. Adv. Manuf. Technol.* **2011**, *57*, 117–125. [\[CrossRef\]](#)
- Yingfei, G.; Jiuhua, X.; Hui, Y. Diamond tools wear and their applicability when ultra-precision turning of SiCp/2009Al matrix composite. *Wear* **2010**, *269*, 699–708. [\[CrossRef\]](#)
- Chen, X.; Liu, C.; Ke, J.; Zhang, J.; Shu, X.; Xu, J. Subsurface damage and phase transformation in laser-assisted nanometric cutting of single crystal silicon. *Mater. Des.* **2020**, *190*, 108524. [\[CrossRef\]](#)
- Zhao, G.; Hu, M.; Li, L.; Zhao, C.; Zhang, J.; Zhang, X. Enhanced machinability of SiCp/Al composites with laser-induced oxidation assisted milling. *Ceram. Int.* **2020**, *46*, 18592–18600. [\[CrossRef\]](#)
- You, K.; Yan, G.; Luo, X.; Gilchrist, M.D.; Fang, F. Advances in laser assisted machining of hard and brittle materials. *J. Manuf. Process.* **2020**, *58*, 677–692. [\[CrossRef\]](#)
- Bertolini, R.; Andrea, G.; Alagan, N.T.; Bruschi, S. Tool wear reduction in ultrasonic vibration-assisted turning of SiC-reinforced metal-matrix composite. *Wear* **2023**, *523*, 204785. [\[CrossRef\]](#)
- Ahmed, F.; Ko, T.J.; Kurniawan, R.; Kwack, Y. Machinability analysis of difficult-to-cut material during ultrasonic vibration-assisted ball end milling. *Mater. Manuf. Process.* **2021**, *36*, 1734–1745. [\[CrossRef\]](#)
- Xing, Y.; Xue, C.; Liu, Y.; Du, H.; Yip, W.S.; To, S. Freeform surfaces manufacturing of optical glass by ultrasonic vibration-assisted slow tool servo turning. *J. Mater. Process. Technol.* **2023**, *324*, 118271. [\[CrossRef\]](#)
- Yin, T.; Du, H.; Zhang, G.; Hang, W.; To, S. Theoretical and experimental investigation into the formation mechanism of surface waviness in ultra-precision grinding. *Tribol. Int.* **2023**, *180*, 108269. [\[CrossRef\]](#)
- Mayer, J.E., Jr.; Fang, G.-P. Effect of grinding parameters on surface finish of ground ceramics. *CIRP Ann.* **1995**, *44*, 279–282. [\[CrossRef\]](#)
- De Souza Ruzzi, R.; da Silva, R.B.; da Silva, L.R.R.; Machado, Á.R.; Jackson, M.J.; Hassui, A. Influence of grinding parameters on Inconel 625 surface grinding. *J. Manuf. Process.* **2020**, *55*, 174–185. [\[CrossRef\]](#)
- Nadolny, K.; Kapłonek, W. Design of a device for precision shaping of grinding wheel macro-and micro-geometry. *J. Cent. South Univ.* **2012**, *19*, 135–143. [\[CrossRef\]](#)
- Wasif, M.; Iqbal, S.A.; Ahmed, A.; Tufail, M.; Rababah, M. Optimization of simplified grinding wheel geometry for the accurate generation of end-mill cutters using the five-axis CNC grinding process. *Int. J. Adv. Manuf. Technol.* **2019**, *105*, 4325–4344. [\[CrossRef\]](#)
- Gopal, A.V.; Rao, P.V. Selection of optimum conditions for maximum material removal rate with surface finish and damage as constraints in SiC grinding. *Int. J. Mach. Tools Manuf.* **2003**, *43*, 1327–1336. [\[CrossRef\]](#)
- Demir, H.; Gullu, A.; Ciftci, I.; Seker, U. An investigation into the influences of grain size and grinding parameters on surface roughness and grinding forces when grinding. *J. Mech. Eng.* **2010**, *56*, 447–454.

23. Yang, M.; Kong, M.; Li, C.; Long, Y.; Zhang, Y.; Sharma, S.; Li, R.; Gao, T.; Liu, M.; Cui, X. Temperature field model in surface grinding: A comparative assessment. *Int. J. Extrem. Manuf.* **2023**, *5*, 042011. [\[CrossRef\]](#)
24. Shen, B.; Shih, A.J.; Tung, S.C. Application of nanofluids in minimum quantity lubrication grinding. *Tribol. Trans.* **2008**, *51*, 730–737. [\[CrossRef\]](#)
25. Wang, Y.; Li, C.; Zhang, Y.; Yang, M.; Li, B.; Dong, L.; Wang, J. Processing characteristics of vegetable oil-based nanofluid MQL for grinding different workpiece materials. *Int. J. Precis. Eng. Manuf. Green Technol.* **2018**, *5*, 327–339. [\[CrossRef\]](#)
26. Daneshi, A.; Jandaghi, N.; Tawakoli, T. Effect of dressing on internal cylindrical grinding. *Procedia CIRP* **2014**, *14*, 37–41. [\[CrossRef\]](#)
27. Hassui, A.; Diniz, A.E. Correlating surface roughness and vibration on plunge cylindrical grinding of steel. *Int. J. Mach. Tools Manuf.* **2003**, *43*, 855–862. [\[CrossRef\]](#)
28. Tang, J.; Du, J.; Chen, Y. Modeling and experimental study of grinding forces in surface grinding. *J. Mater. Process. Technol.* **2009**, *209*, 2847–2854. [\[CrossRef\]](#)
29. Deresse, N.C.; Deshpande, V.; Taifa, I.W. Experimental investigation of the effects of process parameters on material removal rate using Taguchi method in external cylindrical grinding operation. *Eng. Sci. Technol. Int. J.* **2020**, *23*, 405–420. [\[CrossRef\]](#)
30. Nadolny, K.; Kieraś, S. Experimental studies on the centrifugal MQL-CCA method of applying coolant during the internal cylindrical grinding process. *Materials* **2020**, *13*, 2383. [\[CrossRef\]](#)
31. Qin, F.; Zhang, L.; Chen, P.; An, T.; Dai, Y.; Gong, Y.; Yi, Z.; Wang, H. In situ wireless measurement of grinding force in silicon wafer self-rotating grinding process. *Mech. Syst. Signal Process.* **2021**, *154*, 107550. [\[CrossRef\]](#)
32. Wang, Z.; Guo, J. Research on an optimized machining method for parallel grinding of f- θ optics. *Int. J. Adv. Manuf. Technol.* **2015**, *80*, 1411–1419. [\[CrossRef\]](#)
33. Xi, J.; Zhao, H.; Li, B.; Ren, D. Profile error compensation in cross-grinding mode for large-diameter aspheric mirrors. *Int. J. Adv. Manuf. Technol.* **2016**, *83*, 1515–1523. [\[CrossRef\]](#)
34. Patel, A.; Bauer, R.; Warkentin, A. Investigation of the effect of speed ratio on workpiece surface topography and grinding power in cylindrical plunge grinding using grooved and non-grooved grinding wheels. *Int. J. Adv. Manuf. Technol.* **2019**, *105*, 2977–2987. [\[CrossRef\]](#)
35. Chidambaram, S.; Pei, Z.; Kassir, S. Fine grinding of silicon wafers: A mathematical model for grinding marks. *Int. J. Mach. Tools Manuf.* **2003**, *43*, 1595–1602. [\[CrossRef\]](#)
36. Huo, F.; Kang, R.; Li, Z.; Guo, D. Origin, modeling and suppression of grinding marks in ultra precision grinding of silicon wafers. *Int. J. Mach. Tools Manuf.* **2013**, *66*, 54–65. [\[CrossRef\]](#)
37. Wang, T.; Liu, H.; Wu, C.; Cheng, J.; Chen, M. Three-dimensional modeling and theoretical investigation of grinding marks on the surface in small ball-end diamond wheel grinding. *Int. J. Mech. Sci.* **2020**, *173*, 105467. [\[CrossRef\]](#)
38. Sun, X.; Stephenson, D.; Ohnishi, O.; Baldwin, A. An investigation into parallel and cross grinding of BK7 glass. *Precis. Eng.* **2006**, *30*, 145–153. [\[CrossRef\]](#)
39. Pan, Y.; Zhao, Q.; Guo, B.; Chen, B.; Wang, J.; Wu, X. An investigation of the surface waviness features of ground surface in parallel grinding process. *Int. J. Mech. Sci.* **2020**, *170*, 105351. [\[CrossRef\]](#)
40. Chen, B.; Guo, B.; Zhao, Q. An investigation into parallel and cross grinding of aspheric surface on monocrystal silicon. *Int. J. Adv. Manuf. Technol.* **2015**, *80*, 737–746. [\[CrossRef\]](#)
41. Jiang, C.; Guo, Y.; Li, H. Parallel grinding error for a noncoaxial nonaxisymmetric aspheric lens using a fixture with adjustable gradient. *Int. J. Adv. Manuf. Technol.* **2013**, *66*, 537–545. [\[CrossRef\]](#)
42. Chen, S.; Cheung, C.F.; Zhang, F.; Liu, M. Optimization of tool path for uniform scallop-height in ultra-precision grinding of free-form surfaces. *Nanomanuf. Metrol.* **2019**, *2*, 215–224. [\[CrossRef\]](#)
43. Chen, S.; Cheung, C.; Zhao, C.; Zhang, F. Simulated and measured surface roughness in high-speed grinding of silicon carbide wafers. *Int. J. Adv. Manuf. Technol.* **2017**, *91*, 719–730. [\[CrossRef\]](#)
44. Yin, T.; Zhang, G.; Du, J.; To, S. Nonlinear analysis of stability and rotational accuracy of an unbalanced rotor supported by aerostatic journal bearings. *IEEE Access* **2021**, *9*, 61887–61900. [\[CrossRef\]](#)
45. Yin, T.; To, S.; Du, H.; Zhang, G. Effects of wheel spindle error motion on surface generation in grinding. *Int. J. Mech. Sci.* **2022**, *218*, 107046. [\[CrossRef\]](#)
46. Cao, Y.; Guan, J.; Li, B.; Chen, X.; Yang, J.; Gan, C. Modeling and simulation of grinding surface topography considering wheel vibration. *Int. J. Adv. Manuf. Technol.* **2013**, *66*, 937–945. [\[CrossRef\]](#)
47. Badger, J.; Murphy, S.; O'Donnell, G. The effect of wheel eccentricity and run-out on grinding forces, waviness, wheel wear and chatter. *Int. J. Mach. Tools Manuf.* **2011**, *51*, 766–774. [\[CrossRef\]](#)

Disclaimer/Publisher's Note: The statements, opinions and data contained in all publications are solely those of the individual author(s) and contributor(s) and not of MDPI and/or the editor(s). MDPI and/or the editor(s) disclaim responsibility for any injury to people or property resulting from any ideas, methods, instructions or products referred to in the content.